ELSEVIER

Journal of Chromatography A, 702 (1995) 223–231

JOURNAL OF CHROMATOGRAPHY A

Separation of enantiomers of 1*a*,2,7,7*a*-tetrahydro-3-methoxynaphtha-(2,3*b*)-oxirane by liquid chromatography: laboratory-scale elution chromatography and modelling of simulated moving bed

A.E. Rodrigues*, Z.P. Lu, J.M. Loureiro, L.S. Pais

Laboratory of Separation and Reaction Engineering, School of Engineering, University of Porto, 4099 Porto Codex, Portugal

Abstract

The separation of enantiomers of 1*a*,2,7,7*a*-tetrahydro-3-methoxynaphtha-(2,3*b*)-oxirane (Sandoz epoxide) on cellulose triacetate HPLC columns was investigated on the laboratory scale. The performance of the columns was calculated by HEPT measurements and the slopes of the adsorption equilibrium isotherms and effective diffusivities were calculated from elution chromatographic experiments. Multi-component adsorption equilibrium isotherms were calculated from single isotherms by using the ideal adsorbed solution (IAS) model. Simulation of continuous chromatographic separation of the racemic mixture of Sandoz epoxide in a simulated moving bed was carried out and the effect of mass transfer coefficient on process performance was analysed.

1. Introduction

The need for the separation of enantiomers for pharmaceutical applications is increasing as regulatory aspects become more stringent. The separation of enantiomers by HPLC is an active field of research. Many chromatographic packings have been developed and, according to Sheldon [1], can be classified into (a) chiral ligand-exchange phases, (b) affinity phases, (c) helical polymer phases, e.g., cellulose derivatives, (d) cavity phases, e.g., cyclodextrin, and (e) Pirkle-type phases, e.g., amino acid derivatives immobilized on silica by either ionic or covalent attachment.

In many instances these are difficult separations and therefore continuous chromatography should be considered. In the chemical engineering field the concept of the simulated moving bed (SMB) has been known since 1961 when the first patent by Broughton [2] appeared. Many processes are in industrial operations, e.g., Parex for the separation of *p*-xylene and Sarex for the separation of fructose and glucose in the high fructose corn syrup (HFCS) industry.

The application in the pharamceutical and fine chemistry industries is in its infancy, however. It is worth mentioning the development of simulated moving bed units for such applications made by Separex in cooperation with IFP on the pilot and industrial scales.

The operation of SMB units is not as simple as elution, frontal or displacement chromatography. Therefore, understanding how the system reacts to changes in operating parameters is of crucial importance. Modelling and simulation

* Corresponding author.

0021-9673/95/$09.50
SSDI 0021-9673(94)01037-4

studies are of importance before running the system. This requires a knowledge of some basic information on equilibrium and kinetic parameters.

The test system to be studied here is the separation of enantiomers of 1*a*,2,7,7*a*-tetrahydro-3-methoxynaphtha-(2,3*b*)-oxirane (Sandoz expoxide; Sandoz, Basle, Switzerland):

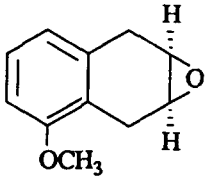

The objectives of this work were (i) to obtain equilibrium and kinetic parameters from elution chromatographic experiments; (ii) to predict multi-component equilibrium from single isotherms; and (iii) to provide a tool for understanding SMB operation.

2. Experimental and results

2.1 Equipment and chemicals

The laboratory-scale HPLC system (Gilson, Villiers le Bel, France) includes three piston pumps (Model 305 master pump and two Model 306 slave pumps with 10 WTI piston pump heads), a Model 117 UV detector with a standard 5 mm path length flow cell, a Model 811C dynamic mixer, a Model 805 manometric module, a Model 202 fraction collector and a IBM PC 386 computer; the system is completely automated.

Two columns of cellulose triacetate (TCA; Merck, Darmstadt, Germany) as stationary phase were used: column A, laboratory packed, 25 cm × 0.46 cm I.D., particle diameter 15–25 μm; column B, Merck 25 cm × 1 cm I.D., particle diameter 10 μm. Column A was prepared from TCA according to the activation procedure described by Dingenen et al. [3]. In fact, active centres of the adsorbent become accessible only after it has been submitted to swelling in boiling methanol. Therefore, 100 g of TCA in 500 ml of methanol were boiled at 80°C under reflux for 30 min. This suspension was allowed to cool at ambient temperature and then decanted in order to eliminate the fines, which would lead to high pressure drops in the column. An HPLC column slurry packer with axial compression to 200 bar was used to pack column A.

The columns used in the simulated moving bed pilot plant were wider (I.D. 2.6 cm, length ca. 9 cm). They were packed according to the procedure described by Nicoud [4].

The mobile phase used was methanol (LiChrosolv; Merck). All runs were carried out at 25°C. The total concentration of the sample (racemic mixture) was 0.25 g/l. The outlet concentration was determined by UV detection at 220 nm; the flow-rates used were in the range 0.1–2 ml/min.

2.2. Elution chromatography

Several elution chromatographic runs were carried out in order to assess the influence of the operating parameters on the column behaviour, namely the effect of flow-rate and particle diameter.

The effect of flow-rate on the separation of enantiomers is shown in Fig. 1 for column A at flow-rates 0.9, 0.5 and 0.1 ml/min. Similar results for column B are shown in Fig. 2 for flow-rates of 2, 0.7 and 0.3 ml/min. As the particle diameter is smaller and the column has a larger cross-sectional area, complete separation of the peaks is achieved even at a flow-rate of 2 ml/min.

2.3. Column performance

The column performance can be characterized by its height equivalent to a theoretical plate (HEPT), which can be calculated from the mean μ_1 and variance σ^2 of a chromatographic peak as $\mathrm{HETP} = \sigma^2 L/\mu_1^2$. The Van Deemter plot, i.e., HETP versus superficial velocity u_0, was calculated from experiments with column A at various flow-rates with the pure (+)-isomer previously separated in the same column from a racemic mixture at 1 g/l; for column B we directly used

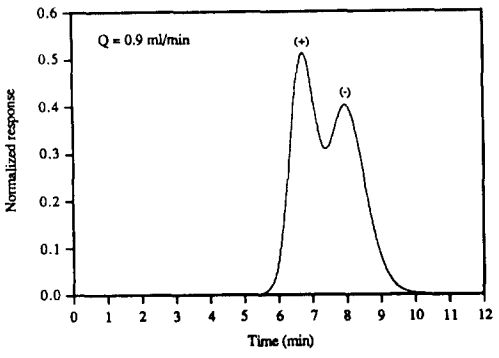

(a)

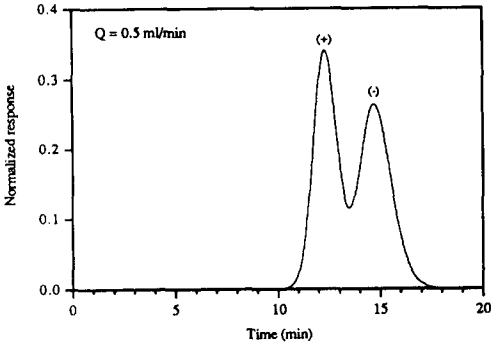

(b)

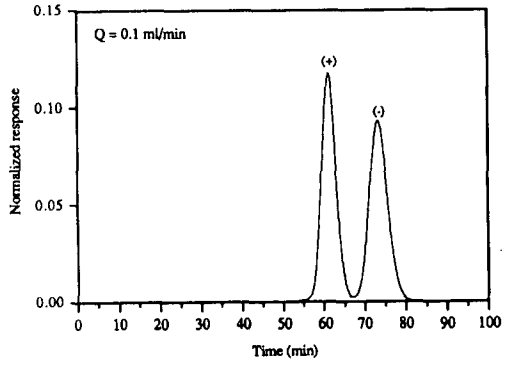

(c)

Fig. 1. Effect of flow-rate on enantiomer separation with column A (25 cm × 0.46 cm I.D.) packed with TCA particles of d_p = 15–25 μm.

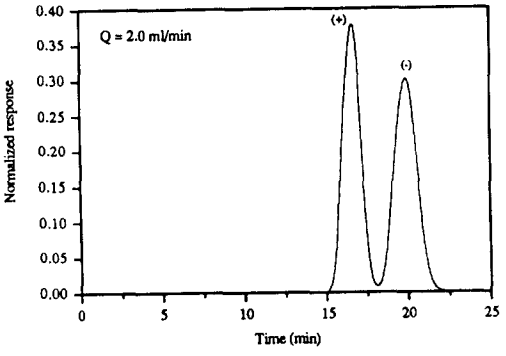

(a)

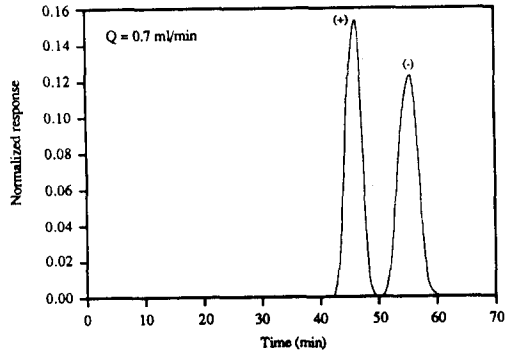

(b)

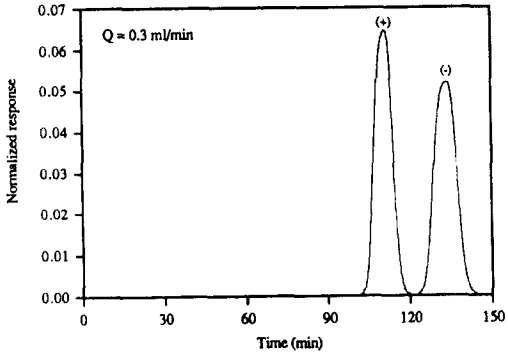

(c)

Fig. 2. Effect of flow-rate on enantiomer separation with column B (25 cm × 1 cm I.D.) packed with TCA particles of d_p = 10 μm.

the experiments in Fig. 2 as the peaks were already well separated.

Fig. 3 shows the experimental results obtained for the (+)-isomer in column A.

Van Deemter plots, i.e., HEPT vs. u_0 for columns A and B are shown in Fig. 4. The performance of a Merck column packed with 15–25-μm particles with a similar structure to the 10-μm particles would be represented by a line located above the curves shown.

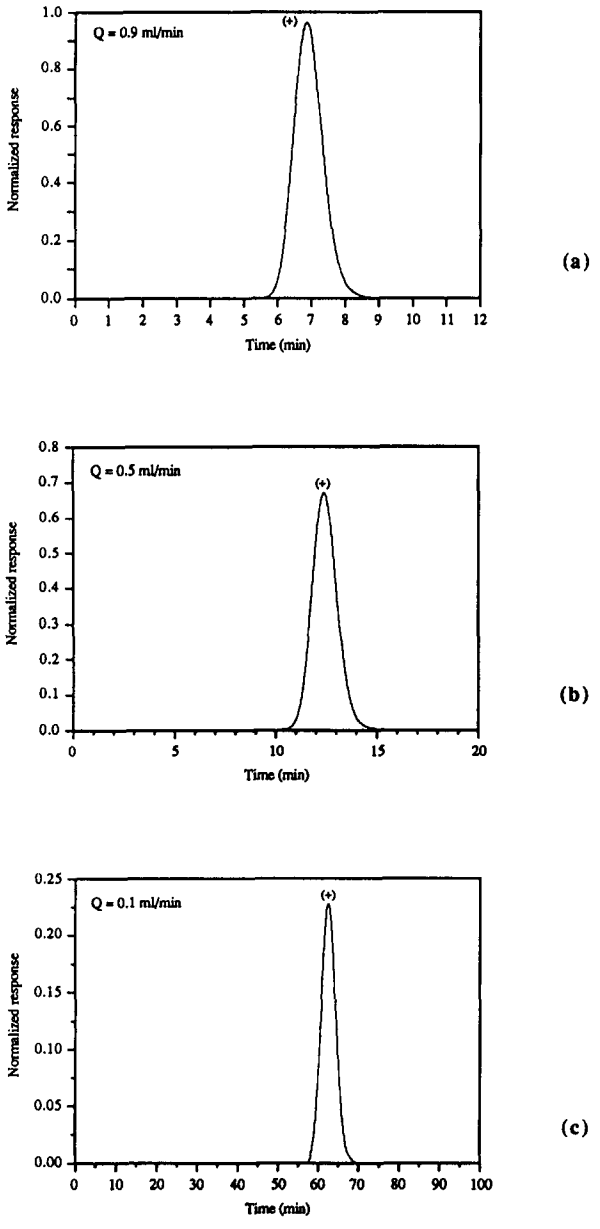

Fig. 3. Effect of flow-rate on the shape of the chromatographic peak of the (+)-isomer with column A.

2.4. Modelling and simulation of elution chromatography

The mathematical model of elution chromatography presented here is based on the following assumptions: homogeneous particle with spherical geometry where mass transport occurs only by diffusion and plug flow with axial dispersion of the outer fluid phase; species i are linearly adsorbed in the particle, i.e., the adsorption equilibrium isotherm relating the adsorbed concentration q_i^* with the bulk fluid phase concentration c_i of species i is $q_i^* = mc_i$. Model equations are then as follows.

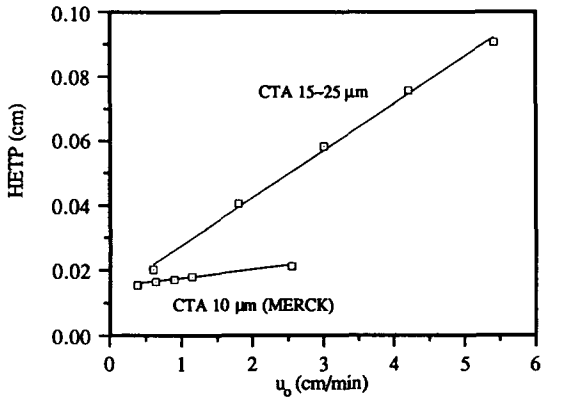

Fig. 4. Van Deemter plots (HETP vs. bed superficial velocity) for both columns.

(a) Mass balance inside particle:

$$\frac{\partial^2 q_i}{\partial \rho^2} + \frac{2}{\rho} \cdot \frac{\partial q_i}{\partial \rho} = \alpha \cdot \frac{\partial q_i}{\partial \theta} \tag{1}$$

with boundary and initial conditions

$$\rho = 0 \qquad \frac{\partial q_i}{\partial \rho} = 0 \qquad \forall \theta \tag{1a}$$

$$\rho = 1 \qquad q_i = q_i^* \qquad \forall \theta \tag{1b}$$

$$\theta = 0 \qquad q_i = 0 \qquad \forall \rho \tag{1c}$$

(b) Adsorption equilibrium isotherm at the liquid–particle interface:

$$q_i^* = mc_i \tag{2}$$

(c) Mass balance in a bed volume element:

$$\frac{1}{Pe} \cdot \frac{\partial^2 c_i}{\partial x^2} - \frac{\partial c_i}{\partial x} - \left(\frac{\partial c_i}{\partial \theta} + \frac{1-\varepsilon}{\varepsilon} \cdot \frac{\partial \langle q_i \rangle}{\partial \theta} \right) = 0 \tag{3}$$

with boundary and initial conditions

$x = 0$ $\quad c_i = M\,\delta(\theta)$ $\quad \forall\theta$ (3a)

$x \to \infty$ $\quad c_i$ limited $\quad \forall\theta$

(open to diffusion boundary) (3b)

$\theta = 0$ $\quad c_i = 0$ $\quad \forall x$ (3c)

In these equations $x = z/L$ is the reduced axial coordinate, $\rho = r/R_p$ is the reduced particle coordinate, $\theta = t/\tau$ is time reduced by the space time $\tau = \varepsilon L/u_0$, ε is the bed porosity, c_i is the concentration in the bulk fluid phase, q_i is the adsorbed concentration in the particle, q_i^* is the adsorbed concentration in equilibrium with c_i, $\langle q_i \rangle$ is the average adsorbed particle concentration and M is the area of the pulse injected into the column. The model parameters are as follows:

$Pe = \dfrac{u_0 L}{\varepsilon D_{ax}}$ Peclet number, ratio of bulk convective and diffusive fluxes;

$\alpha = \dfrac{\tau_d}{\tau}$ ratio of diffusion time constant and space time;

space time;

$k' = \dfrac{1-\varepsilon}{\varepsilon} \cdot m$ adsorption capacity factor;

where $\tau_d = R_p^2/\mathcal{D}_h$ is the time constant for intraparticle diffusion.

2.5. Transfer function of the fixed bed

The transfer function $G(s)$ of the fixed bed is obtained by solving the resulting system of PDEs with Laplace transformation, i.e.,

$$G(s) = \exp\left\{\frac{Pe}{2} \cdot \left[1 - \sqrt{1 + \frac{4N(s)}{Pe}}\right]\right\} \tag{4}$$

where

$$N(s) = s[1 + k'M(s)] \tag{5}$$

and

$$M(s) = \frac{3}{\sqrt{\alpha s}} \cdot \left(\frac{1}{\tanh\sqrt{\alpha s}} - \frac{1}{\alpha s}\right) \tag{6}$$

2.6. Moments of the impulse response

The moments of the impulse response are obtained from the Van der Laan relationship:

$$\mu_n = (-1)^n \left.\frac{\partial^n G(s)}{\partial s^n}\right|_{s=0} \tag{7}$$

and so

$$\mu_1 = 1 + k' \tag{7a}$$

$$\mu_2 = \frac{2}{15} \cdot k'\alpha + \left(1 + \frac{2}{Pe}\right) \cdot (1 + k')^2 \tag{7b}$$

The mean of the peak is located at a time equal to $\mu_1\tau$. The variance $\sigma^2 = \mu_2 - \mu_1^2$ measures the contribution of all dispersive phenomena and is given by

$$\sigma^2 = \frac{2}{Pe}(1 + k')^2 + \frac{2}{15} \cdot k'\alpha \tag{7c}$$

The HETP is

$$\mathrm{HETP} = \frac{\sigma^2 L}{\mu_1^2} = \frac{2L}{Pe} + \frac{2}{15} \cdot \frac{k'\alpha L}{(1 + k')^2} \tag{8}$$

or as a function of the superficial velocity u_0

$$\mathrm{HETP} = \frac{2\varepsilon D_{ax}}{u_0} + \frac{2}{15} \cdot \frac{k'}{\varepsilon} \frac{\tau_d}{(1 + k')^2} \cdot u_0 \tag{8a}$$

2.7. Analysing results

Experimental results with the (+)-isomer in columns A and B are summarized in Tables 1 and 2, respectively.

From Table 1 we obtain the slope of the adsorption equilibrium isotherm of the (+)-iso-

Table 1
Elution chromatography: experimental results with column A (laboratory packed)

Q (ml/min)	$\tau\mu_{1,\mathrm{exp}}$ (min)	$\tau^2\sigma^2_{,\mathrm{exp}}$ (min^2)	m_{exp}
0.9	6.93	0.17	1.83
0.7	8.89	0.24	1.83
0.5	12.46	0.36	1.83
0.3	20.73	0.70	1.83
0.1	62.77	3.19	1.85

$\varepsilon = 0.4$; column volume = 4.15 ml.

Table 2
Elution chromatography: experimental results with column B (Merck)

Q (ml/min)	$\tau\mu_{1,exp}$ (min)	$\tau^2\sigma^2_{,exp}$ (min^2)	m_{exp}
2.0	16.59	0.24	2.15
0.9	35.72	0.92	2.06
0.7	45.90	1.45	2.06
0.5	64.38	2.73	2.06
0.3	110.65	7.58	2.15

$\varepsilon = 0.4$; column volume = 19.63 ml.

mer in the linear region $m = 1.83$, in agreement with that reported by Nicoud and co-workers [5,6]. From Table 2 the average value of $m = 2.10$ from column B is around 15% higher than that obtained in column A.

Simulations of experiments in column A with the (+)-isomer alone were carried out by using fast Fourier transformation to invert the transfer function $G(s)$, Eq. 4. In these simulations we used $m(+) = 1.83$ and the molecular diffusivity $\mathcal{D}_m = 5 \cdot 10^{-6}$ cm^2/s of the (+)-isomer estimated with the Wilke–Chang correlation, where the ligand molar volume was calculated by Schroeder's method [7]. With the above value of $\mathcal{D}_m$ the Peclet number Pe was calculated by the following correlation with $\gamma_1 = 20$ and $\gamma_2 = 0.5$:

$$\frac{1}{Pe} = \frac{\varepsilon\gamma_1\mathcal{D}_m}{u_0 L} + \varepsilon\gamma_2 \cdot \frac{d_p}{L} \qquad (9)$$

Simulation and experimental results are compared in Fig. 5 using for all runs $\tau_d = 0.2525$ min or $\mathcal{D}_h = 6.6 \cdot 10^{-8}$ cm^2/s. The mean deviation in variance between the theoretical and experimental values is around 24%.

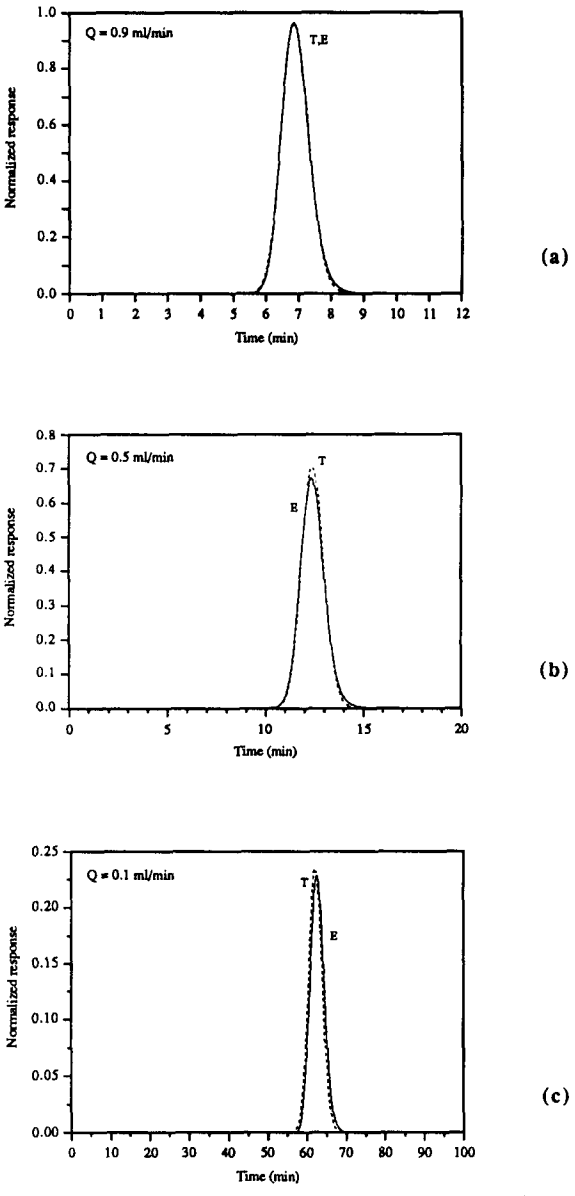

Fig. 5. Comparison between experimental (solid lines) and model (dashed lines) results for elution chromatography of the (+)-isomer with column A.

2.8. Continuous chromatography in a simulated moving bed

The SMB technology was applied to the separation of optical isomers by Negawa and Shoji [8]. The pilot-scale simulated moving bed (Licosep 12/26 [9,10]) is shown schematically in Fig. 6. It consists of twelve columns of 10×2.6 cm I.D.; the locations of the feed, extract and raffinate streams move clockwise. The rotation period is an important parameter for the operation of the SMB. The package developed for the SMB [11] considers a plug-dispersive model for bulk fluid phase flow and a linear intraparticle driving force (LDF) model for the particle equations, containing one parameter k (mass

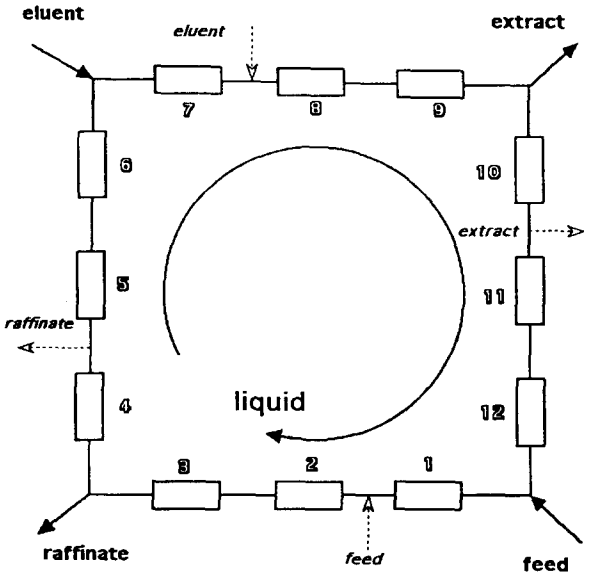

Fig. 6. Schematic representation of the Licosep simulated moving bed unit.

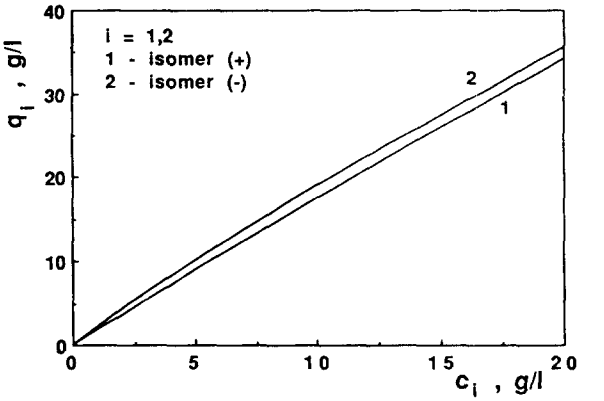

Fig. 7. Single-component adsorption equilibrium isotherms.

transfer coefficient). At this level approximations for "homogeneous" and "pore diffusion" equations can be included. For linear systems they are just linked by $1 + \xi_p$, where ξ_p is the particle capacity factor.

For packings containing large pores where intraparticle convection occurs the LDF still holds provided we consider the augmented mass transfer coefficient $\tilde{k} = k/f(\lambda)$, where [12]

$$f(\lambda) = \frac{3}{\lambda}\left(\frac{1}{\tanh \lambda} - \frac{1}{\lambda}\right)$$

and $\lambda = v_0 R_p / 3De$ is the intraparticle Peclet number.

The multi-component adsorption equilibrium isotherm was calculated from the single isotherms shown in Fig. 7 by using the ideal adsorbed solution (IAS) model [13,14], which leads to the results shown in Fig. 8.

Single adsorption isotherms of isomers on TCA are given by a linear + Langmuir equation:

$$q_i^0 = mc_i^0 + \frac{Qb_i c_i^0}{1 + b_i c_i^0} \qquad (10)$$

where the superscript zero refers to single-component adsorption, Q is the maximum langmuirian adsorbed concentration, equal for both isomers, and b_i are the respective Langmuir adsorption constants.

The prediction of multi-component equilib-

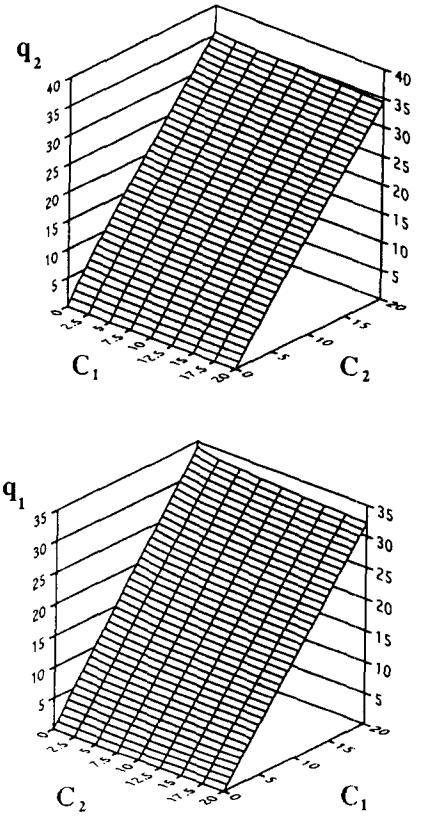

Fig. 8. Multi-component adsorption equilibrium isotherms for both enantiomers predicted by the IAS model.

rium with the IAS model involves iterative calculation with the following system of equations:

$$c_i = c_i^0(\pi_i, T)z_i \tag{11}$$

$$q_i^* = \frac{z_i}{\sum_{i=1}^{N} z_i/q_i^0} \tag{12}$$

$$\pi_i = \frac{\mathcal{R}T}{\sigma}\int_0^{c_i^0} \frac{q_i^0}{c_i^0}\,dc_i^0 \tag{13}$$

$$\sum_{i=1}^{N} z_i = 1 \tag{14}$$

In these equations, q_i^* is the adsorbed concentration of enantiomer i in equilibrium with c_i in the mixture, and q_i^0 and c_i^0, related by Eq. 10, are the respective concentrations in a corresponding (same modified spreading pressure) single-component system, z_i is the surface coverage mole fraction of component i, π_i is the spreading pressure of isomer i on the surface, σ is the surface area per unit weight of adsorbent, T is the absolute temperature and $\mathcal{R}$ is the perfect gas constant.

Simulated results for the SMB for the set of parameters shown in Table 3 are presented in Fig. 9. These results show the effect of the mass transfer coefficient k in the process performance. It is clearly seen that purity of the isomers recovered in the extract and raffinate streams increases with k. Therefore, in packings where intraparticle convection is important we expect a better performance for a given system operating under given conditions.

Table 3
Values of the parameters used in simulations of the SMB

Eluent flow-rate (ml/min)	4.53
Raffinate flow-rate (ml/min)	2.05
Extract flow-rate (ml/min)	4.00
Feed (ml/min)	1.52
Recycle flow-rate (ml/min)	20.35
Rotation period (s)	260
Feed concentrations of A and B (g/l)	5
Mass transfer coefficient k (s^{-1})	0.05–0.2

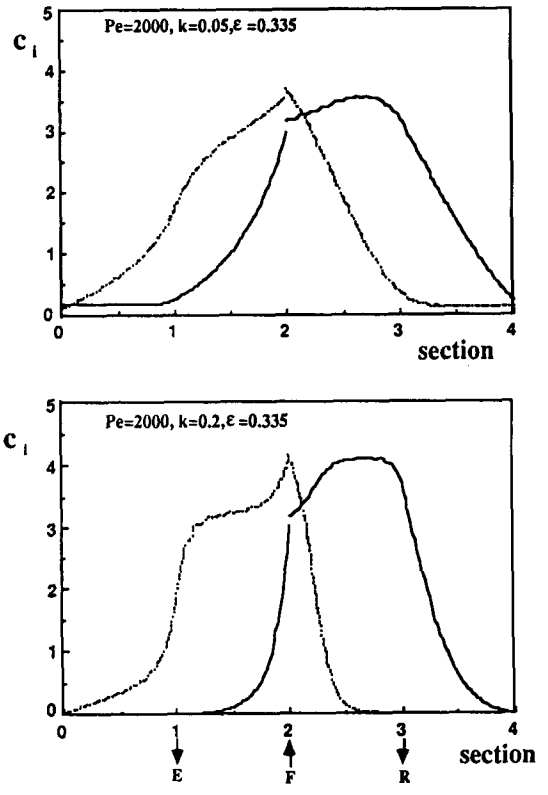

Fig. 9. Effect of the mass transfer coefficient k on the cyclic steady-state concentration profiles in an SMB unit.

3. Conclusions

We have considered the methodology for characterization of packings used in the chromatographic separation of optical isomers. Equilibrium and kinetic parameters (effective diffusivity) were obtained from laboratory elution chromatographic experiments.

From single-component adsorption equilibrium isotherms, multi-component equilibrium data were calculated based on the ideal adsorbed solution (IAS) model.

A model of the simulated moving bed (SMB) allowed the understanding of its operation; the effect of the mass transfer coefficient k on the performance of the system was studied; it has been shown that with increasing k (reducing intraparticle resistances), the performance improves.

Acknowledgements

The European Community under the BRITE-EURAM Programme (Contract no. BRE2-CT92-0337) is thanked for financial support and the staff of Separex for helpful discussions.

Symbols

c_i	fluid phase concentration of component i
c_i^0	fluid phase concentration of component i in a single-component system
d_p	particle diameter
D_{ax}	axial dispersion coefficient
D_e	effective diffusivity
$\mathscr{D}_h$	intraparticle diffusivity
$\mathscr{D}_m$	molecular diffusivity
k	mass transfer coefficient
$\tilde{k}$	augmented (by intraparticle convection) mass transfer coefficient
k'	column adsorption capacity factor
L	column length
m	slope of the linear adsorption isotherm
M	area of the injected pulse
Pe	bed Peclet number
q_i	adsorbed (solid-phase) concentration of component i
q_i^0	adsorbed concentration of species i in equilibrium with c_i^0 in a single-component system
q_i^*	adsorbed concentration of species i in equilibrium with c_i
$\langle q_i \rangle$	average adsorbed concentration of species i
r	particle coordinate
$\mathscr{R}$	perfect gas constant
R_p	particle radius
T	absolute temperature
u_0	bed superficial velocity
v_0	intraparticle superficial velocity
x	reduced axial coordinate in column
z	axial coordinate in column
z_i	surface coverage mole fraction of component i

Greek symbols

α	ratio of diffusion time constant and space time
$\delta(\theta)$	Dirac delta function
ε	bed porosity
γ_1, γ_2	parameters in the correlation for Pe
λ	intraparticle Peclet number
μ_n	moment of order n of the impulse response
π_i	spreading pressure of component i on the adsorbent surface
θ	time reduced by space time
ρ	reduced particle coordinate
σ	surface area per unit mass of adsorbent
σ^2	variance of the chromatographic peak
τ	space time
τ_d	diffusion time constant
ξ_p	particle capacity factor

References

[1] R. Sheldon. *Chirotechnology*, Marcel Dekker, New York, 1983.
[2] D. Broughton, *US Pat.*, 2 985 589 (1961).
[3] J. Dingenen, I. Somers, F. Pavwels and A. Van Loon, in M. Perrut (Editor), *Proceedings of the 9th International Symposium on Preparative and Industrial Chromatography*, Société Française de Chimie, Paris, 1992.
[4] R.M. Nicoud, *LC·GC Int.*, 6 (1993) 636–637.
[5] R.M. Nicoud, G. Fuchs, E. Küsters, R. Reuille and E. Schmid, presented at the *3rd International Symposium on Chiral Discrimination*, Tübingen, 5–8 October, 1992.
[6] G. Fuchs, R.M. Nicoud and M. Bailly, in M. Perrut (Editor), *Proceedings of the 9th International Symposium on Preparative and Industrial Chromatography*, Société Française de Chimie, Paris, 1992.
[7] R.C. Reid, J.M. Prausnitz and B.E. Poling, *The Properties of Gases and Liquids*, McGraw-Hill. New York, 4th ed., 1987.
[8] M. Negawa and F. Shoji, *J. Chromatogr.*, 590 (1992) 113–117.
[9] R.M. Nicoud, *LC·GC Int.*, 5 (1992) 43–47.
[10] B. Balannec and G. Hottier, in G. Ganetsos and P. Barker (Editors), *Preparative and Production Scale Chromatography*, Marcel Dekker, New York, 1992.
[11] A.E. Rodrigues, Z.P. Lu, J.M. Loureiro and L.S. Pais, in preparation.
[12] A.E. Rodrigues, B. Ahn and A. Zoulalian, *AIChE J.*, 28 (1982) 541.
[13] A. Myers and J. Prausnitz, *AIChE J.*, 11 (1965) 121.
[14] D. Frey and A.E. Rodrigues, *AIChE J.*, 40 (1994) 182.